Supporting Information

Hierarchical Iron-Nickel Oxyhydroxide Nanosheets on Porous $TiFe_2$-based Intermetallics for Robust Oxygen Evolution

Qian Zhao, Zhenli He, Yuehui He, Yue Qiu, Zhonghe Wang and Yao Jiang*

State Key Laboratory of Powder Metallurgy, Powder Metallurgy Research Institute, Central South University, Changsha 410083, China.

E-mail: jiangyao@csu.edu.cn (Y. Jiang)

Experimental section

Materials

Fe powder (D_{50} = 25.9 μm, 99.9 %), Ti powder (D_{50} = 28.7 μm, 99.9 %) and Ni powder (D_{50} = 25.9 μm, 99.9 %) were purchased from Beijing Xing Rong Yuan Technology Co. Ltd. (China, Beijing). KOH (≥ 85%) was obtained from Sinopharm Chemical Reagent Co. Ltd. (China, Shanghai). All the chemical reagents were commercially available and analytical grade, and used without any further treatment.

Synthesis of porous $TiFe_2$-based intermetallics

In a typical synthesis process of porous $TiFe_2$-based intermetallics, they were synthesized by the reaction of Ti, Fe, and Ni elemental powders. Porous $TiFe_2$-based intermetallics with various amounts of Ni contents (2 at.%, 4 at.%, 6 at.%, 10 at.%, 15 at.%, and 20 at.%, denote as $TiFe_2$-2Ni, $TiFe_2$-4Ni, $TiFe_2$-6Ni, $TiFe_2$-10Ni, $TiFe_2$-15Ni, and $TiFe_2$-20Ni, respectively) were prepared in the same method. The powders were mixed in different ratios for 48 h and loosely placed in a corundum sintering boat (60 × 10 mm), and then put in a vacuum furnace for pressureless sintering. The sintering process involves warming and cooling processes. The warming stages of $TiFe_2$, $TiFe_2$-2Ni, $TiFe_2$-4Ni, $TiFe_2$-6Ni and $TiFe_2$-10Ni were held at 120 °C, 400 °C, 600 °C, 900 °C, 1100 °C, and 1250 °C, while the warming stages of $TiFe_2$-15Ni and $TiFe_2$-20Ni were held at 120 °C, 400 °C, 600 °C, 900 °C, and 1100 °C in order to avoid the liquid phase during the sintering process. The cooling stages of all samples were held at 900 °C and 600 °C to reduce the thermal stress generated during the rapid cooling of the material. During the sintering process, the heating rate was ≤5 °C min^{-1} when the temperature was below 1000 °C and ≤2 °C min^{-1} when the temperature was above 1000 °C and the vacuum was kept below 1×10^{-3} Pa.

Synthesis of iron-nickel nanosheets on porous $TiFe_2$-based intermetallics

The prepared porous $TiFe_2$-based intermetallics were polished to a rectangular shape with a width of 1 cm and a length of more than 2 cm. After washing and drying, samples are soaked in 1 M KOH solution for 12h at 50 °C for alkali corrosion (AC), then washed with deionized water and anhydrous ethanol and dried for further usage. The XRD patterns of the powders treated with AC for 12 h at 50 °C shows insignificant change compared with the XRD patterns of those before treatment, which is due to the fact that nanosheets formed on the surface is so thin and in small proportions, making it difficult to characterize. In order to investigate the formation of nanosheets, the prepared porous $TiFe_2$ and $TiFe_2$-20Ni were broken into powders by high-energy ball milling for 12 h, and the powders were treated for 144 h at 50 °C. Then the powders were washed with deionized water and anhydrous ethanol and dried for XRD and TEM tests.

Physical and chemical characterization

The crystal phases of samples are revealed by the X-ray diffractometer (XRD, Rigaku D/Max 2500) recorded on a Rigaku D/Max 2500 diffractometer with Cu Kα (λ = 0.15406 nm) as the radiation source. The microstructure and pore structure of porous $TiFe_2$-based intermetallics were observed by field emission scanning electron microscope (FESEM, MIRA 3), and the compositions of the samples were analyzed by energy-dispersive X-ray spectroscope (EDS) attached to the FESEM instrument. Transmission electron microscopy (TEM) are used to characterize the phases and morphology of the nanosheets and the bonding of nanosheets and the substrate (FEI TF20). X-ray photoelectron spectroscopy (XPS) was tested by ESCALABSB 250 Xi equipment with Al Kα X-ray radiation as the excitation source. The open porosity was measured by the Archimedes method.

Electrochemical characterization

The electrochemical measurements were carried out in a standard three-electrode cell system (CHI660D). The saturated calomel electrode (SCE) and platinum plate with a 1.0 cm^2 surface were used as the reference and counter electrode, respectively. KOH solution (1.0 M) was used as the electrolyte. The as-obtained electrodes were used as the working electrodes (1 × 1 cm). When preparing the commercial RuO_2 electrodes, 10 mg RuO_2 powder was ultrasonically dispersed in a mixture of 965 μL isopropanol and 35 μL of 5 wt.% Nafion solution. The ink solution is then sonicated for 30 min to get a uniform suspension. Then, 10 μl of the catalyst ink is deposited on the glassy carbon (3 mm in diameter) substrate to obtain a loading of 1.415 mg cm^{-2}. Linear sweep voltammetry (LSV) was carried out at a scan rate of 1 mV s^{-1}, and the working electrodes were activated by the LSV test several times until the curves were stable before the LSV tests. All polarization curves were corrected with the iR in this work, and all potentials in this study are converted to the reversible hydrogen electrode (RHE) reference scale by E(RHE) = E(SCE) + 0.059pH + 0.244. Tafel plots were obtained from the polarization curves (overpotential (η) versus the logarithm of current density (log |J|)). Electrochemical impedance spectroscopy (EIS) analysis was performed in a frequency range from 0.01 Hz to 10^5 Hz. Cyclic voltammograms (CVs) with various scan rates were used to estimate the double-layer capacitance. The halves of the positive and negative current density at the center of the scanning range with different scan rates were plotted, and the slopes represent the double-layer capacitance. Accelerated durability tests of catalysts were performed by continuous potential cycling between -0.4 ~ 0.5 V vs. SCE at a scan rate of 100 mV s^{-1} for 5000 cycles. The chronopotentiometry tests were performed for 50 h at a constant current density of 100 mA cm^{-2}. Turnover frequency (TOF) is calculated to estimate the intrinsic catalytic ability of the nanosheets on $TiFe_2$-20Ni. The CVs were recorded in 1 mol/L KOH by sweeping the potential between 1.15 and 1.55 Vs RHE with scan rates of 10, 20, 30, 40 and 50 mV s^{-1}(Figure R2a and Supplementary Figure S15a). TOF was calculated by the equation: slope = $n^2F^2m/4RT$ (n = 1, is hypothesizing a one-electron oxidation process of metal centers; F = 96485 C mol^{-1}, is the

Faradaic constant; m is the number of active species; R = 8.314 J $mol^{-1}K^{-1}$, is the ideal gas constant and the absolute temperature for T = 298 K), we can utilize the operated value of m in another formula: TOF = jA/4Fm (j is the current density; A = 1 cm^{-2}, is the geometrical electrode area; 4 represents the number of electrons needed to evolve one molecule of O_2).

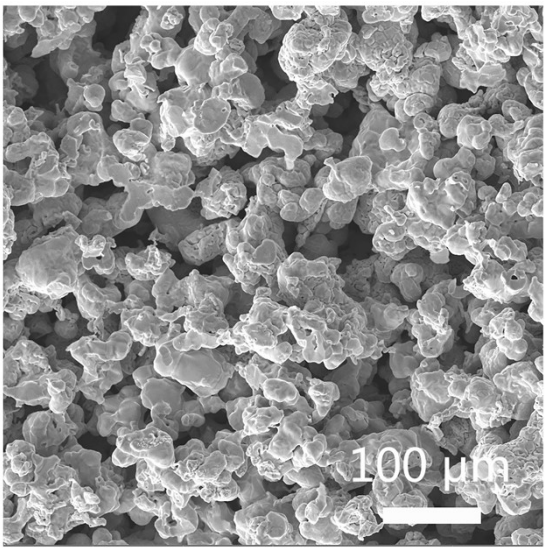

Figure S1. SEM image of the porous $TiFe_2$ intermetallic.

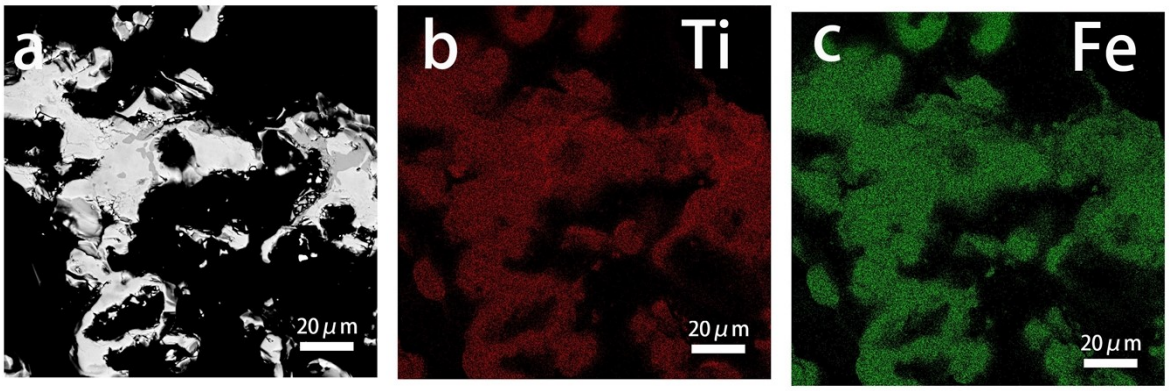

Figure S2. The corresponding elemental mapping images of the porous $TiFe_2$ intermetallic.

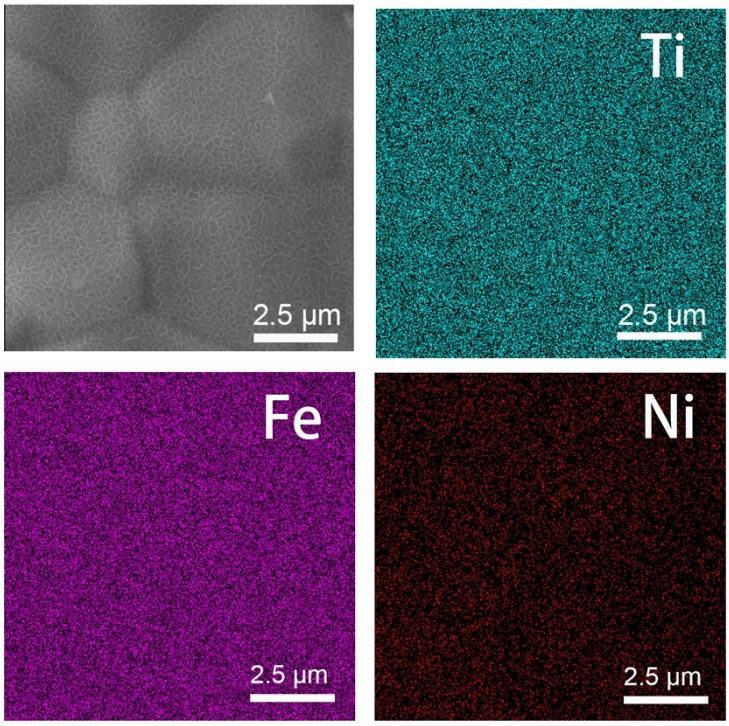

Figure S3. The corresponding elemental mapping images of nanosheets on porous $TiFe_2$-20Ni.

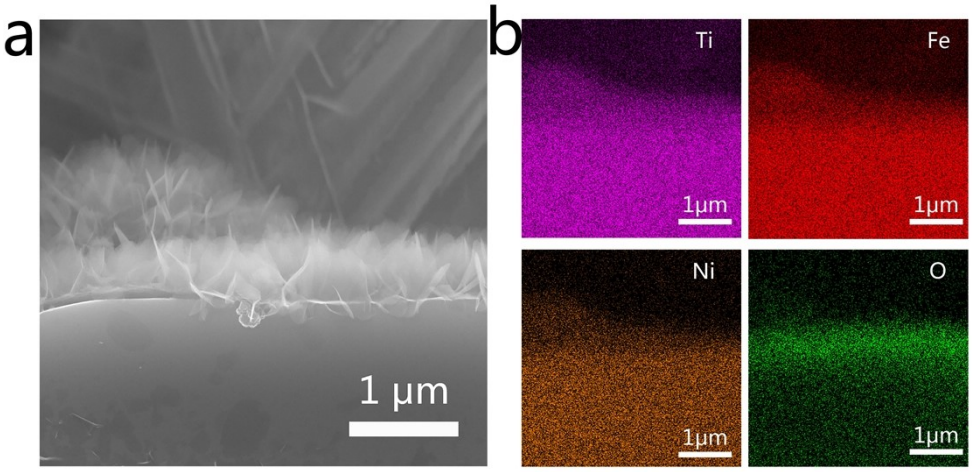

Figure S4. The corresponding elemental mapping images of nanosheets on porous $TiFe_2$-20Ni.

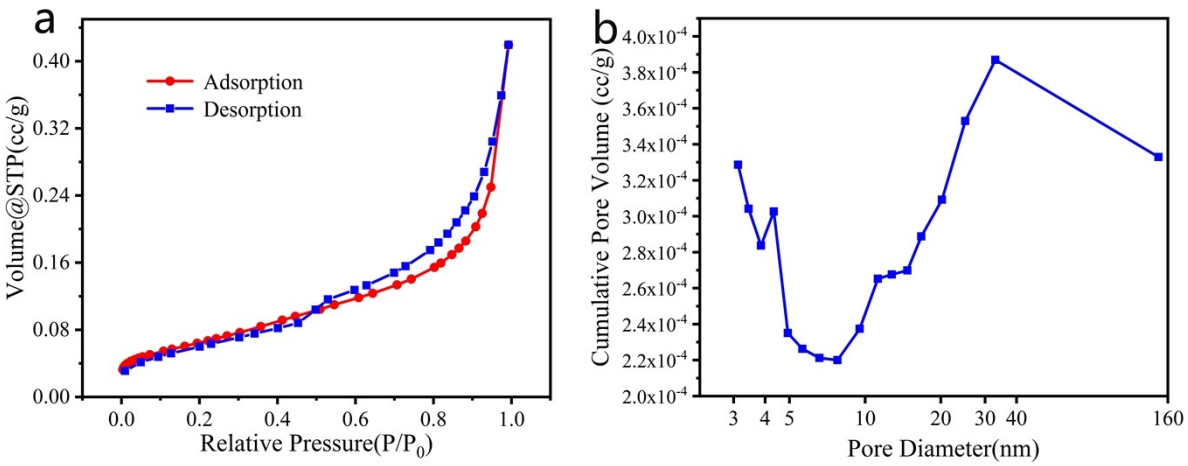

Figure S5. a)The N_2 Adsorption-desorption isotherm. b) The pore distribution of nanosheets on $TiFe_2$-20Ni.

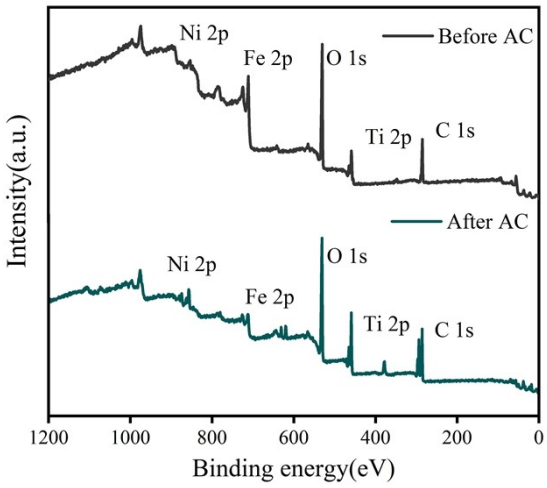

Figure S6. XPS spectra of porous $TiFe_2$-20Ni before and after AC.

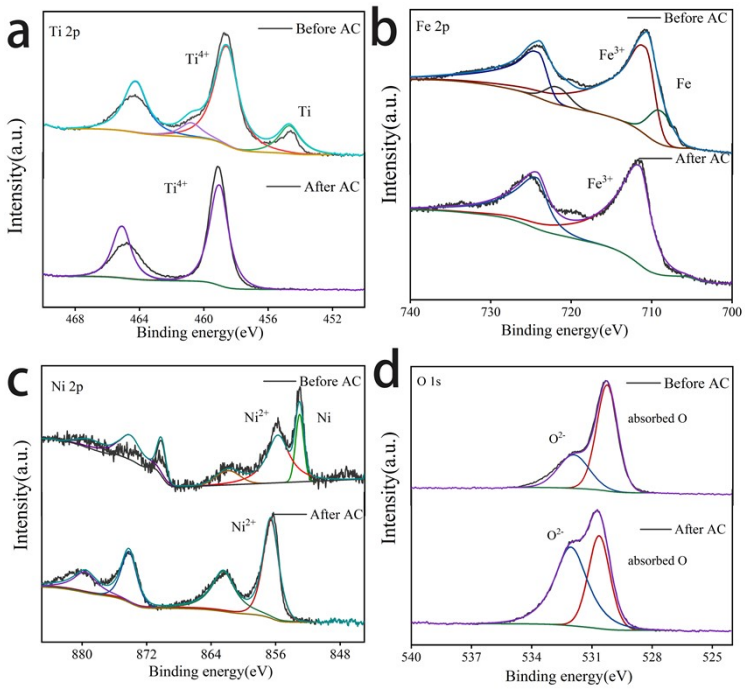

Figure S7. XPS spectra of the nanosheets on Ni-doped $TiFe_2$-based intermetallics. a) Ti 2p. b) Fe 2p. c) Ni 2p. d) O 1s.

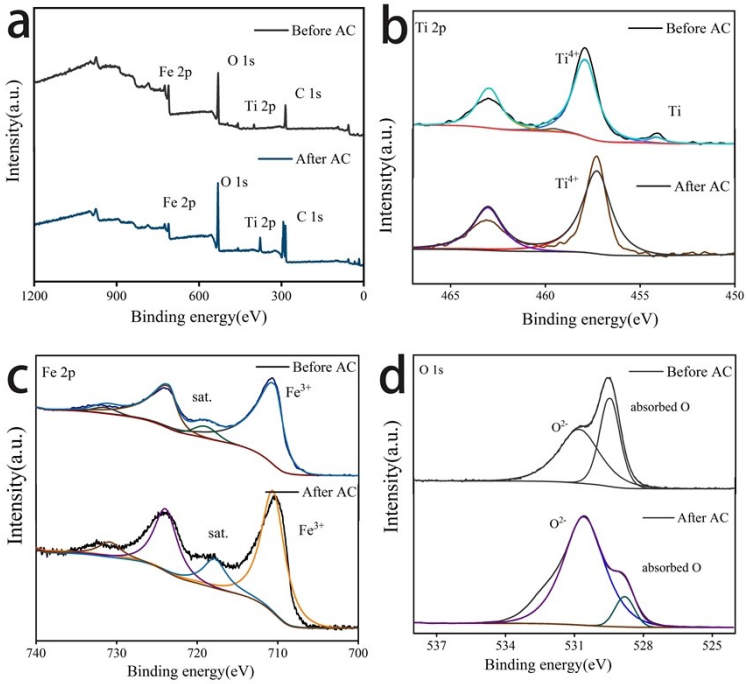

Figure S8. XPS spectra of porous $TiFe_2$ before and after AC. a) survey. b) Ti 2p. c) Fe 2p. d) O 1s.

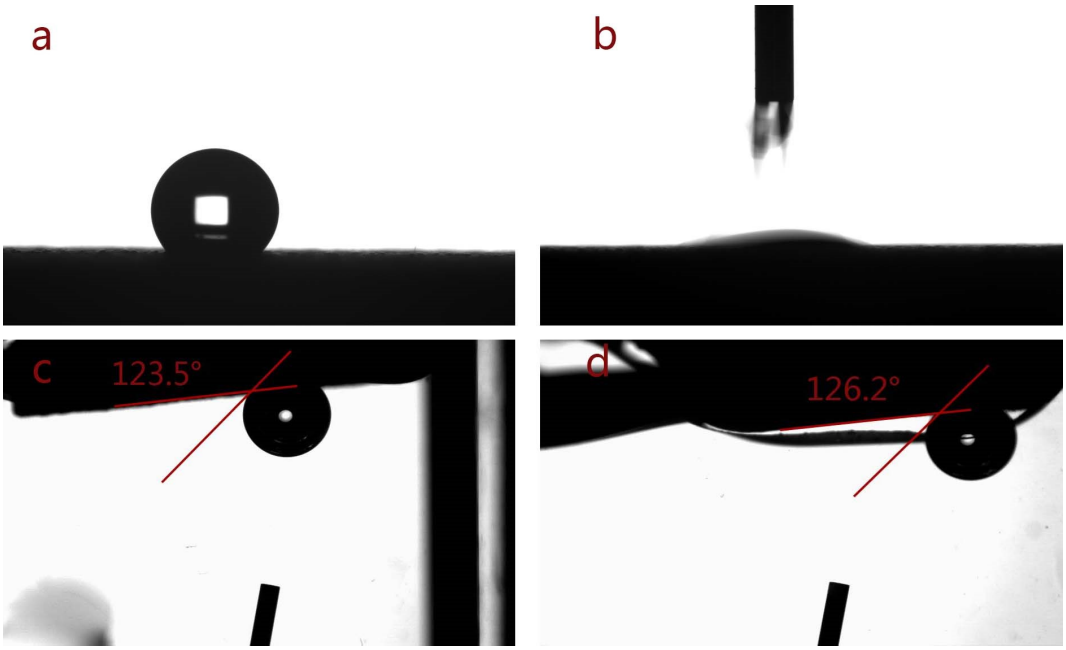

Figure S9. a) The water contact angle of $TiFe_2$-20Ni without nanosheets. b) The water contact angle of nanosheets on $TiFe_2$-20Ni. c) The bubble contact angle of $TiFe_2$-20Ni without nanosheets. d) The bubble contact angle of nanosheets on $TiFe_2$-20Ni.

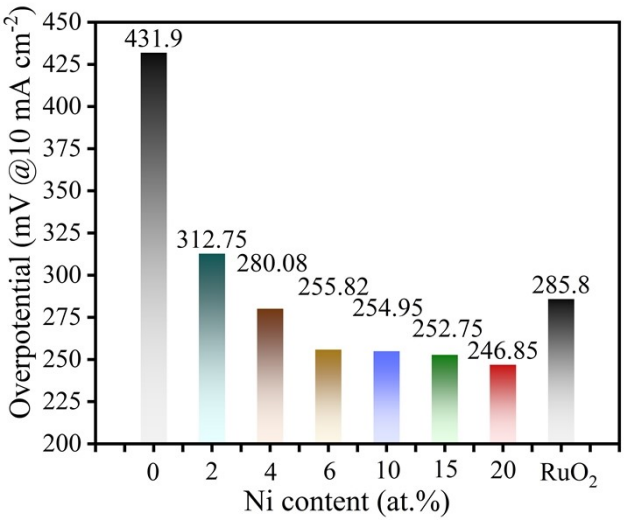

Figure S10. Overpotentials of the nanosheets on Ni-doped $TiFe_2$ and RuO_2.

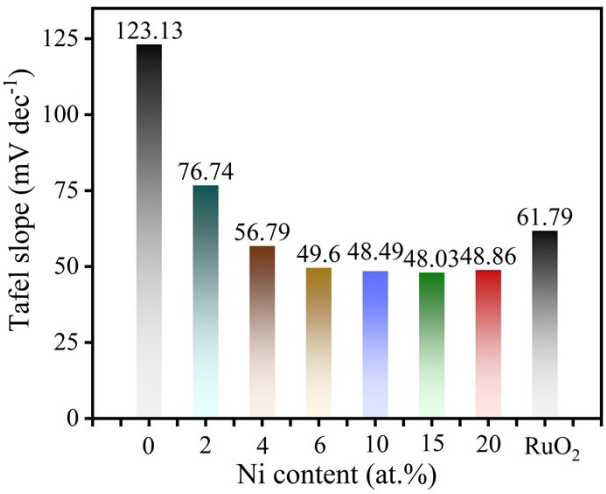

Figure S11. Tafel slopes of the nanosheets on Ni-doped $TiFe_2$ and RuO_2.

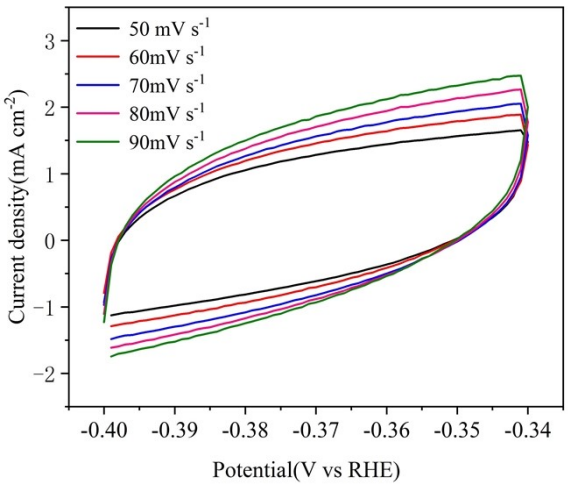

Figure S12. CVs of the nanosheets on porous $TiFe_2$ in the non-faradaic capacitance current range.

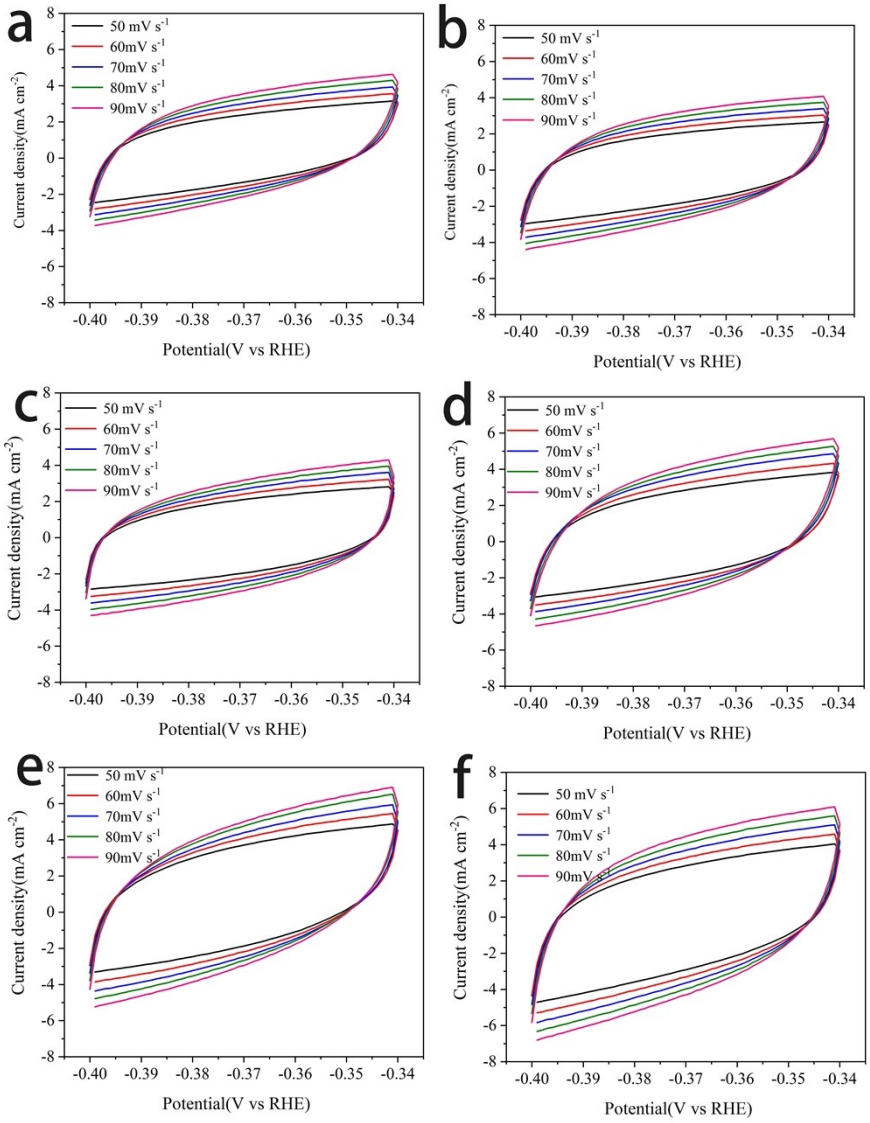

Figure S13. CVs of the nanosheets on porous $TiFe_2$-based intermetallics with different amount of Ni in the non-faradaic capacitance current range. a) Nanosheets on $TiFe_2$-2Ni. b) Nanosheets on $TiFe_2$-4Ni. c) Nanosheets on $TiFe_2$-6Ni. d) Nanosheets on $TiFe_2$-10Ni. e) Nanosheets on $TiFe_2$-15Ni. f) Nanosheets on $TiFe_2$-20Ni.

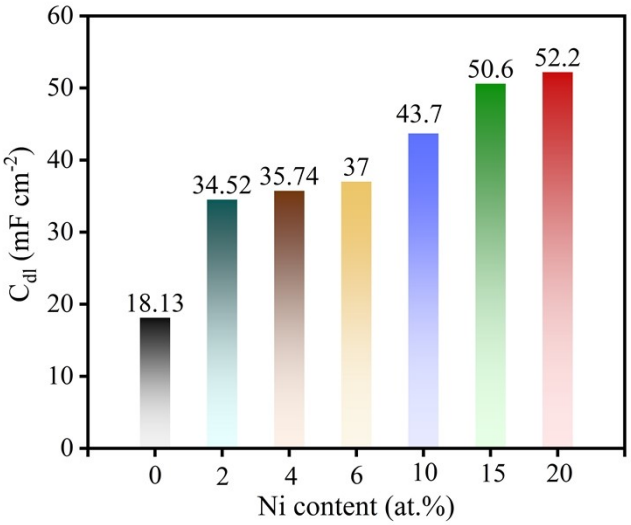

Figure S14. C_{dl} of the nanosheets on Ni-doped $TiFe_2$.

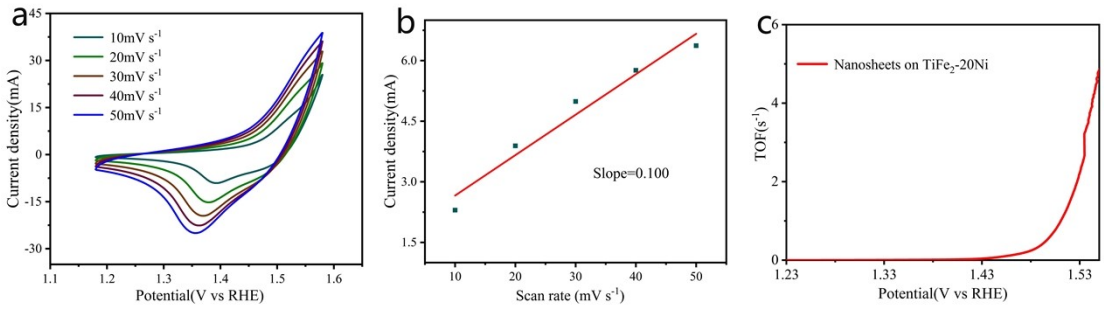

Figure S15. a) CV of nanosheets on $TiFe_2$-20Ni at different scanning rates. b) Corresponding linear graph of scanning rates versus oxidation peak current. c) The TOF profiles vs overpotential of nanosheets on $TiFe_2$-20Ni.

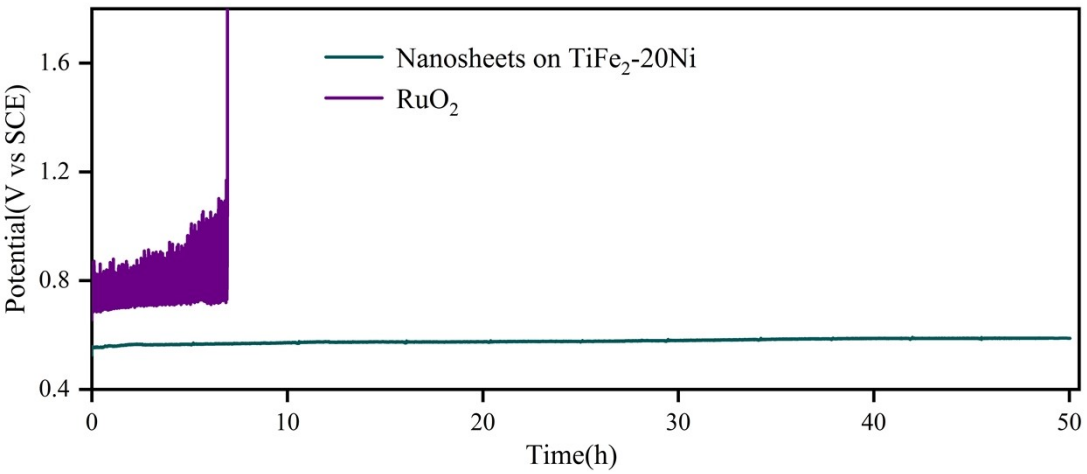

Figure S16. Chronopotentiometry curves of nanosheets on $TiFe_2$-20Ni and RuO_2 at 100 mA cm^{-2}.

Table S1. Electrochemical parameters obtained from EIS tests.

Samples	R_s ($\Omega \cdot cm^2$)	CPE_1 (F /cm^2)	R_p ($\Omega \cdot cm^2$)
Nanosheets on $TiFe_2$	1.016	0.0444	125.8
Nanosheets on $TiFe_2$-2Ni	0.631	0.00685	65.3
Nanosheets on $TiFe_2$-4Ni	0.3996	0.0234	41.18
Nanosheets on $TiFe_2$-6Ni	0.655	0.0491	28.73
Nanosheets on $TiFe_2$-10Ni	0.735	0.0814	7.666
Nanosheets on $TiFe_2$-15Ni	0.635	0.280	3.679
Nanosheets on $TiFe_2$-20Ni	1.04	0.180	3.287

Table S2. Comparisons of the OER activity of nanosheets on porous $TiFe_2$-20Ni with other recently reported catalysts. (@ 10 mA cm^{-2})

Catalyst	Overpotential(mV) @10 mA cm^{-2}	Tafel slope (mV dec^{-1})	Reference
Nanosheets on Porous $TiFe_2$-20Ni	246.85	48.86	This work
RuO_2	285.80	61.79	This work
M-PCBN/CC	232	32	(1)
Ag NW@NiMn-LDHs	270	40.2	(2)
$CoCeNiFeZnCuO_x$	211	21	(3)
CoNi-LDH@PCPs	350	58	(4)
$(NiCo)_3Se_4$(NiCoOOH)	268	42	(5)
NiFeP@NPC	350	78	(6)
Ni–Fe–Se nanocage	249	36	(7)
ECA-CNS	290	46	(8)
NiCoFeB nanochains	284	46	(9)
γ-FeOOH/NF-6M	286	51	(10)
Ni–Fe–Mg	310	150	(11)
Au-$Ni(OH)_2$	288	55	(12)
Fe-Co9S8@CoO	296	65	(13)
FeOOH(Se)/IF	287	54	(14)
$Co_5Fe_3Cr_2$ (oxy)hydroxide	232	-	(15)

Table S3. Comparisons of the OER activity of nanosheets on porous $TiFe_2$-20Ni with other recently reported catalysts. (@ 100 mA cm^{-2})

Catalyst	Overpotential(mV)@100 mA cm^{-2}	Reference
Nanosheets on Porous $TiFe_2$-20Ni	295	This work
NiHCF/$Ni(OH)_2$	289	(16)
Fe–N–$CoSe_2$	290	(17)
Cu_2Se/$NiSe_2$/NF	290	(18)
FeCoNiMo HEA/C	300	(19)
$Ni3Fe_{0.9}Cr_{0.1}$/CACC	302	(20)
Fe-Co_3O_4	303	(21)
CoCeNiFeZnCuO_x	307	(22)
Sn–$Ni(OH)_2$	312	(23)
$NiFe_{0.05}$–N–CP	320	(24)
NiCo-H/NF	331	(25)
MoO_3/Ni–NiO	347	(26)
γ-FeOOH&NF	362	(10)
meso-$CoFe_{0.05}O_x$	373	(27)
B-TS-H@T-B	419.4	(28)
FCNSNP	427	(29)

Supplementary References

1. R. Abazari, S. Sanati and A. Morsali, *Inorg. Chem.* 2022, **61**, 3396-3405.
2. S. A. Chala, M. C. Tsai, W. N. Su, K. B. Ibrahim, B. Thirumalraj, T. S. Chan, J. Lee, H. Dai and B.-j. Hwang, *ACS Nano*, 2020. **14.** 1770-1782.
3. G. Li, L. Lu, L. Pei, Z. Ma, Y. Yuan, M.-L. Hu, Q. Miao and J. Zhong, *Inorg. Chem.* 2022, **61**, 738-745.
4. W. Wang, Y. Lu, M. Zhao, R. Luo, Y. Yang, T. Peng, H. Yan, X. Liu and Y. Luo, *ACS Nano*, 2019, **13**, 12206-12218.
5. J. Abed, S. Ahmadi, L. Laverdure, A. M. Abdellah, C. P. O'Brien, K. M. Cole, P. H. Sobrinho, D. Sinton, D. C. Higgins, N. J. Mosey, S. J. Thorpe and E. H. Sargent, *Adv. Mater.* 2021, **33**. 2103812.
6. J. Wang and F. Ciucci, *Appl. Catal. B* 2019, **254**, 292-299.
7. Z.-P. Wu, X. F. Lu, S.-Q. Zang and X. W. Lou, *Adv. Funct. Mater*. 2020, **30**, 1910274.
8. Y.-R. Hong, S. Mhin, K.-M. Kim, W.-S. Han, H. Choi, G. Ali, K. Y. Chung, H. J. Lee, S.-I. Moon, S. Dutta, S. Sun, Y.-G. Jung, T. Song and H. Han, *J. Mater. Chem. A*, 2019, **7**, 3592-3602.
9. Y. Li, B. Huang, Y. Sun, M. Luo, Y. Yang, Y. Qin, L. Wang, C. Li, F. Lv, W. Zhang and S. Guo, *Small*, 2019, **15**, 1804212.
10. K. Wang, H. Du, S. He, L. Liu, K. Yang, J. Sun, Y. Liu, Z. Du, L. Xie, W. Ai and W. Huang, *Adv. Mater.* 2021, **33**. 2005587.
11. N. Wang, Z. Cao, X. Zheng, B. Zhang and E. H. Sargent, *Adv. Mater.* 2020, **32**. 1906806.
12. R. Madhu, A. Karmakar, K. Karthick, S. Sam Sankar, S. Kumaravel, K. Bera and S. Kundu, *Inorg. Chem.* 2021, **60**, 15818-15829.
13. T. Wang, C. Li, X. Liao, Q. Li, W. Hu, Y. Chen, W. Yuan and H. Lin, *Int. J. Hydrog. Energy.* 2022, **47**, 21182-21190.
14. S. Niu, W.-J. Jiang, Z. Wei, T. Tang, J. Ma, J.-S. Hu and L.-J. Wan, *J. Am. Chem. Soc.* 2019, **141**, 7005-7013.
15. K. Bera, R. Madhu, H. N. Dhandapani, S. Nagappan, A. De and S. Kundu, *Inorg. Chem.* 2022, **61**, 16895-16904.
16. W. Hua, H. Sun, M. Jiang, L. Ren, Y. Zhang and J.-G. Wang, *J. Mater. Chem. A*, 2022, **10**, 7366-7372.
17. D. Li, Y. Xing, C. Zhou, Y. Lu, S. Xu, X. Shi, D. Jiang and W. Shi, *Inorg. Chem. Front.* 2021, **8**, 2725-2734.
18. R. Bose, K. Karuppasamy, P. Arunkumar, G. K. Veerasubramani, S. Gayathri, P. Santhoshkumar, D. Vikraman, J. H. Han, H.-S. Kim and A. Alfantazi, *ACS Sustain. Chem. Eng.* 2021, **9**, 13114-13123.
19. Y. Mei, Y. Feng, C. Zhang, Y. Zhang, Q. Qi and J. Hu, *ACS Catal.* 2022, **12**, 10808-10817.
20. J. Zheng, J. Zhang, L. Zhang, W. Zhang, X. Wang, Z. Cui, H. Song, Z. Liang and L. Du, *ACS Appl. Mater. Interfaces.* 2022, **14**, 19524-19533.
21. S. L. Zhang, B. Y. Guan, X. F. Lu, S. Xi, Y. Du and X. Lou, *Adv. Mater.* 2020, **32.** 2002235..
22. W. Huang, J. Zhang, D. Liu, W. Xu, Y. Wang, J. Yao, H. T. Tan, K. N. Dinh, C. Wu, M. Kuang, W. Fang, R. Dangol, L. Song, K. Zhou, C. Liu, J. W. Xu, B. Liu and Q. Yan, *ACS Nano*, 2020, **14**, 17640-17651.
23. J. Jian, X. Kou, H. Wang, L. Chang, L. Zhang, S. Gao, Y. Xu and H. Yuan, *ACS Appl. Mater. Interfaces.* 2021, **13**, 42861-42869.
24. Y. Xu, Z. Cheng, J. Jiang, J. Du and Q. Xu, *ChemComm,* 2021, **57**, 13170-13173.
25. M. Chen, D. Liu, J. Feng, P. Zhou, L. Qiao, W. Feng, Y. Chen, K. Wei Ng, S. Wang, W. Fai Ip and H. Pan, *Chem. Eng. J.* 2022, **443**, 136432.
26. X. Li, Y. Wang, J. Wang, Y. Da, J. Zhang, L. Li, C. Zhong, Y. Deng, X. Han and W. Hu, *Adv. Mater.* 2020, **32**. 2003414.
27. T. Tang, Q. Zhang, X. Bai, Z. Wang and J. Guan, *ChemComm,* 2021, **57**, 11843-11846.
28. T. Li, T. Jing, D. Rao, X. Jia, Y. Zuo, Š. Kment and R. Zbořil, *J. Mater. Chem. A*, 2021, **9**, 12283-12290.
29. M. B. Z. Hegazy, K. Harrath, D. Tetzlaff, M. Smialkowski, D. Siegmund, J. Li, R. Cao and U.-P. Apfel, *iScience*, 2022, **25**, 105148.